Supplementary Material

In this Supplementary Material, we investigate more sophisticated networks with multiple RISs and IOs as well as practical issues.

1 DOPPLER AND MULTIPATH FADING EFFECTS: CASE STUDIES WITH MULTIPLE REFLECTORS

In this supplementary section, we extend our system models and analyses in sections 2 and 3 into propagation scenarios with multiple IOs with and without intelligent reflection capabilities. We follow a bottom-up approach starting with two IOs and illustrate the fading/Doppler effect mitigation capabilities of RISs. We also propose a number of effective and novel methods with different functionalities.

1.1 Direct Signal and Two Reflected Signals without any RISs

In this subsection, by extending our model given in section 2, we consider the propagation scenario of **Figure S1** with two IOs. Here, in order to spice up our analyses, we assume that while the BS-MS and BS-IO 1-MS links are parallel to the ground, the reflected signal from IO 2 arrives to the MS with an angle of α with respect to the MS route. In this scenario, the initial (horizontal) distances between the BS and the MS, the MS and IO 1, and the MS and IO 2 are shown by d_{LOS}, d_1, and d_2, respectively. Using a similar analysis as in section 2, under the assumption of unit gain reflection coefficients for both IOs, that is $R_1 = R_2 = -1$, the time-varying received complex envelope can be expressed as

$$r(t) = \frac{\lambda}{4\pi}\left(\frac{e^{-j2\pi f_D t}}{d_{\text{LOS}}} - \frac{e^{j2\pi f_D t}}{d_{\text{LOS}} + 2d_1} - \frac{e^{j2\pi f_D (\cos\alpha) t - j\phi_2}}{\tilde{d}_2}\right) \tag{S1}$$

where $\tilde{d}_2 = \sqrt{d_2^2 \tan^2\alpha + (d_{\text{LOS}} + d_2)^2} + d_2/(\cos\alpha)$ is the initial radio path distance for the reflected signal of IO 2, which is obtained after simple trigonometric operations, and $\phi_2 = 2\pi\tilde{d}_2/\lambda$ is a fixed phase term. Here, we assume that the variations in terms of the large-scale path loss due to the movement of MS are almost negligible (as in **Figure 1**) and the rays from IO 2 remain parallel for all points of the mobile route, which corresponds to radio path distance decrements of $Vt\cos\alpha$, with respect to time, for these rays. It is worth noting that parallel ray assumption is approximately true for short route lengths (Goldsmith, 2005). As seen from (S1), the received signal has three Doppler components: $-f_D$ Hz, f_D Hz, and $f_D\cos\alpha$ Hz due to the rays coming from the BS, IO 1, and IO 2, respectively.

In **Figure S2**, we show the magnitude of the complex envelope as well as the Doppler spectrum for the case of $\alpha = 60°$, $d_{\text{LOS}} = d_1 = 1000$ m, and $d_2 = 500$ m. As seen from **Figure S2**, due to constructive and destructive interference of the direct and two reflected signals with different Doppler frequency shifts (-100 Hz, 100 Hz, and 50 Hz), the magnitude of the complex envelope exhibits a more hostile and faster fading pattern compared to the simpler scenario of **Figure 1** (see *Figure 2*, top-left subplot).

1.2 Direct Signal and Two Reflected Signals with One or Two RISs

In this subsection, we again focus on the scenario of **Figure S1**, however, under the assumption of one or two RISs that are attached to the existing IOs. Although being more challenging in terms of system

optimization and analysis, we focus on the case of a single RIS first, then extend our analysis into the case of two RISs.

1.2.1 One RIS

Let us assume that we have a single RIS that is mounted on the facade of IO 1 for the scenario of **Figure S1**. For this case, the received complex envelope can be expressed as

$$r(t) = \frac{\lambda}{4\pi}\left(\frac{e^{-j2\pi f_D t}}{d_{\text{LOS}}} + \frac{e^{j2\pi f_D t + j\theta_1(t)}}{d_{\text{LOS}} + 2d_1} - \frac{e^{j2\pi f_D(\cos\alpha)t - j\phi_2}}{\tilde{d}_2}\right). \tag{S2}$$

Here, we assumed that the intelligent reflection from IO 1 is characterized by $\theta_1(t)$. We investigate the following three methods for the adjustment of $\theta_1(t)$, where the corresponding complex envelope magnitudes and Doppler spectrums are shown in **Figure S3** for $\alpha = 60°$, $d_{\text{LOS}} = d_1 = 1000$ m, and $d_2 = 500$ m:

- Method 1: $\theta_1(t) = -4\pi f_D t \pmod{2\pi}$
- Method 2: $\theta_1(t) = 2\pi f_D t(\cos\alpha - 1) - \phi_2 + \pi \pmod{2\pi}$
- Method 3: $\theta_1(t) = 2\pi f_D t(\cos\alpha - 1) - \phi_2 \pmod{2\pi}$

In the first method, we intuitively align the reflected signal from the RIS to the LOS signal. As seen from **Figure S3**, although this adjustment eliminates the 100 Hz component in the spectrum and reduces the Doppler spread compared to the case without RIS (**Figure S2**), we still observe two components in the spectrum and a noticeable fade pattern for the received signal due to uncontrollable reflection through IO 2. It is worth noting that this might be the preferred option to obtain a high time average for the complex envelope magnitude with the price of a high Doppler spread (faster time variation).

In the second method, we align the reflected signal from the RIS to the one from IO 2, however, this worsens the situation by increasing the relative power of the 50 Hz component in the Doppler spectrum. As seen from **Figure S3**, a more severe fade pattern is observed for Method 2 due to destructive interference of the reflected signals to the LOS signal. This would be a preferred option in case of an eavesdropper to degrade its signal quality.

In the third method, we follow a clever approach and instead of aligning our RIS-assisted reflected signal to the existing two signals, we target to eliminate the uncontrollable reflection from IO 2 by out-phasing the reflected two signals. This results a remarkable improvement in both Doppler spectrum and the received complex envelope by almost mitigating the fade pattern. In other words, the RIS scarifies itself in Method 3 to eliminate the uncontrollable reflection from IO 2, which significantly reduces the multipath effect, while a minor variation is still observed due to different radio path lengths of these two signals. More specifically, for the selection of $\theta_1(t)$ in Method 3, we obtain

$$r(t) = \frac{\lambda}{4\pi}\left(\frac{e^{-j2\pi f_D t}}{d_{\text{LOS}}} + e^{j2\pi f_D(\cos\alpha)t - j\phi_2}\left(\frac{1}{d_{\text{LOS}} + 2d_1} - \frac{1}{\tilde{d}_2}\right)\right) \tag{S3}$$

which contains two components. However, the Doppler spread can be remarkably reduced when the radio path distances of the signals reflected from IO 1 and 2, i.e., $d_{\text{LOS}} + 2d_1$ and $\tilde{d}_2$, are close to each other. For instance, for the considered system parameters of d_{LOS}, d_1, d_2, and α in **Figure S3**, we have $\frac{1}{d_{\text{LOS}}} \gg \left(\frac{1}{d_{\text{LOS}}+2d_1} - \frac{1}{\tilde{d}_2}\right)$, which results almost a single-tone received signal $r(t) \approx \frac{\lambda}{4\pi}\left(\frac{e^{-j2\pi f_D t}}{d_{\text{LOS}}}\right)$. This is also evident from the Doppler spectrum of the received signal for Method 3. However, Method 3 cannot guarantee the highest complex envelope magnitude, which is also observed from **Figure S3**.

To gain further insights, in **Figure S4**, we plot the 3D magnitude of the complex envelope with respect to time and varying $\theta_1(t)$ values between 0 and 2π. As seen from **Figure S4**, due to constructive and destructive interference of multipath components (particularly due to the interference of the signal reflected from IO 2), the complex envelope exhibits several deep fades. We also observe that it is not feasible to fix the complex envelope magnitude to its maximum value (-48.69 dB for this specific setup) as in the case of single reflection since the incoming three signals cannot be fully aligned at all times. Finally, we note that performing an exhaustive search for the determination of the optimum reflection phase that maximizes $|r(t)|$ for each time sample might be possible with different system parameters, however, this does not fit within the scope of this study, which explores effective solutions for the RIS configuration. We also verify from **Figure S4** that Method 1 achieves approximately the maximum magnitude for the complex envelope in the considered experiment. In light of our discussion above, we give the following remark:

Remark 5: For the case of two reflections with a single RIS in **Figure S1**, the heuristic choice to maximize the magnitude of the complex envelope is to align the reflected signal to the stronger component, that is, the LOS signal (Method 1) under normal circumstances. While this ensures a very high magnitude for the complex envelope, we still observe a fade pattern in time domain. On the other hand, the RIS can be reversely aligned to the reflected signal from the plain IO (Method 3) to reduce the Doppler spread at the price of a slight degradation in the magnitude of the complex envelope.

Remark 6: For the setup of **Figure S1**, the optimal reflection phase that maximizes the magnitude of the complex envelope is given by

$$\theta_1(t) = \frac{\pi}{2}(1 - \mathrm{sgn}(A)) - \tan^{-1}(-B/A) \tag{S4}$$

where $\mathrm{sgn}(\cdot)$ is the sign function and

$$\begin{aligned} A =& \frac{1}{d_{\mathrm{LOS}}} \cos(4\pi f_D t) - \frac{1}{\tilde{d}_2} \cos(2\pi f_D (1 - \cos\alpha) t + \phi_2) \\ B =& \frac{-1}{d_{\mathrm{LOS}}} \sin(4\pi f_D t) + \frac{1}{\tilde{d}_2} \sin(2\pi f_D (1 - \cos\alpha) t + \phi_2). \end{aligned} \tag{S5}$$

The proof of (S4) is given in Appendix. In **Figure S5**, we compare the reflection phases as well as magnitudes of the complex envelope for Method 1 and the optimum method for the same system parameters. As seen from **Figure S5**, Method 1 provides a very close phase behavior compared to the optimal one due to the stronger LOS path and a very minor degradation can be observed in the magnitude of the complex envelope. Nevertheless, the optimal reflection phase in (S4) is valid for all possible system parameters in **Figure S1** and guarantees the maximum complex envelope magnitude at all times. For reference, magnitude values are also shown in the same figure for Method 3. As seen from **Figure S5**, Method 3 reduces the severity of the fade pattern (Doppler spread) while ensuring the same minimum magnitude at the price of a lower time average for the complex envelope.

1.2.2 Two RISs

Under the assumption of two RISs attached to the existing two IOs in the system of **Figure S1**, the received complex envelope is obtained as

$$r(t) = \frac{\lambda}{4\pi}\left(\frac{e^{-j2\pi f_D t}}{d_{\text{LOS}}} + \frac{e^{j2\pi f_D t + j\theta_1(t)}}{d_{\text{LOS}} + 2d_1} + \frac{e^{j2\pi f_D(\cos\alpha)t - j\phi_2 + j\theta_2(t)}}{\tilde{d}_2}\right) \tag{S6}$$

where the time-varying and intelligent reflection characteristics of RIS 1 and 2 are captured by $\theta_1(t)$ and $\theta_2(t)$, respectively. Here, compared to the previous case, we have more freedom with two controllable reflections and the magnitude of the received signal can be maximized (and the Doppler spread can be minimized) by readily aligning the reflected signals to the LOS signal. This can be done by setting $\theta_1(t) = -4\pi f_D t \pmod{2\pi}$ and $\theta_2(t) = -2\pi f_D t(1+\cos\alpha) + \phi_2 \pmod{2\pi}$, which results

$$r(t) = \frac{\lambda e^{-j2\pi f_D t}}{4\pi}\left(\frac{1}{d_{\text{LOS}}} + \frac{1}{d_{\text{LOS}} + 2d_1} + \frac{1}{\tilde{d}_2}\right). \tag{S7}$$

Similar to the case with single intelligent reflection (subsection 2.2), we obtain a constant-amplitude complex envelope and a minimized Doppler spread (with a single component at $-f_D$ Hz) due to the clever co-phasing of the multipath components. Interested readers may easily obtain the magnitude and the Doppler spectrum of the complex envelope to verify our findings.

1.3 Two RISs without a LOS path

Finally, we extend our analysis for the case of non-LOS transmission through two RISs, which yields

$$r(t) = \frac{\lambda}{4\pi}\left(\frac{e^{j2\pi f_D t + j\theta_1(t)}}{d_{\text{LOS}} + 2d_1} + \frac{e^{j2\pi f_D(\cos\alpha)t - j\phi_2 + j\theta_2(t)}}{\tilde{d}_2}\right). \tag{S8}$$

Similar to the case in section 3, by carefully adjusting the phases of two RISs, the Doppler effect can be totally eliminated due to the nonexistence of the LOS signal, which is out of control of the RISs. It is evident that this can be done by $\theta_1(t) = -2\pi f_D t \pmod{2\pi}$ and $\theta_2(t) = -2\pi f_D(\cos\alpha)t + \phi_2 \pmod{2\pi}$.

1.4 The General Case with Multiple IOs and the Direct Signal

Against this background, in this subsection, we extend our analyses for the general case of **Figure S6**, which consists of a total of R IOs. Here, we assume that N of them are coated with RISs, while the remaining $M = R - N$ ones are plain IOs, which create uncontrollable specular reflections towards the MS. In this scenario (N RISs and M plain IOs), the received complex envelope is given by

$$r(t) = \frac{\lambda}{4\pi}\left(\frac{e^{-j2\pi f_D t}}{d_{\text{LOS}}} + \sum_{i=1}^{N}\frac{e^{j2\pi f_{R,i}t - j\psi_i + j\theta_i(t)}}{\tilde{d}_{R,i}} - \sum_{k=1}^{M}\frac{e^{j2\pi f_{I,k}t - j\phi_k}}{\tilde{d}_{I,k}}\right). \tag{S9}$$

Here, we assume that all rays stemming from IOs remain parallel during the movement of the MS for a short period of time, which is a valid assumption, and without loss of generality, we consider a reflection coefficient of -1 for the plain IOs. Additionally, the corresponding terms in (S9) are defined as follows:

- $f_{R,i}$: Doppler shift for the ith RIS

- $f_{I,k}$: Doppler shift for the kth plain IO
- ψ_i: Constant phase shift for the ith RIS
- ϕ_k: Constant phase shift for the kth plain IO
- $\tilde{d}_{R,i}$: Initial radio path distance for the ith RIS
- $\tilde{d}_{I,k}$: Initial radio path distance for the kth plain IO
- $\theta_i(t)$: Adjustable phase shift of the ith RIS

Here, the Doppler shifts of the RISs and plain IOs are not only dependent on the speed of the MS, but also on their relative positions with respect to the MS, i.e., angles of arrival for the incoming signals: $f_{R,i} = f_D \cos\alpha_i$ and $f_{I,k} = f_D \cos\beta_k$, where α_i and β_k are the angles of arrival for the reflected signals of ith RIS and kth plain IO, respectively. In this generalized scenario, we focus on the following two setups:

1.4.1 Setup I ($\boldsymbol{N \leq M}$)

In this setup, we have more number of uncontrollable reflectors (plain IOs) than RISs. Consequently, we extend our methods in Supplementary subsection 1.2 and target either directly aligning N RISs to the LOS path (to improve the received signal strength) or eliminating the reflections stemming from N out of M plain IOs (to reduce the Doppler spread). While the alignment of the reflected signals to the LOS signal is straightforward (Method 1), the assignment of N RISs to corresponding IOs in real-time appears as an interesting design problem. For this purpose, we consider a brute-force search algorithm to determine the most effective set of IOs to be targeted by RISs (Methods 2 & 3). More specifically, N out of M IOs can be selected in $C(M,N)$ different ways, where $C(\cdot,\cdot)$ is the binomial coefficient. Since these N RISs can be assigned to N plain IOs in $N!$ ways, we obtain a total of $P(M,N) = C(M,N)N!$ possibilities (permutations) for the assignment of N RISs to M IOs. Our methodology has been summarized below:

- Method 1: We align the existing N RISs to the LOS path by adjusting their reflection phases as $\theta_i(t) = -2\pi f_{R,i}t + \psi_i - 2\pi f_D t \pmod{2\pi}$ for $i = 1, 2, \ldots, N$.
- Method 2: For the ith RIS minimizing the effect of the reflection stemming from the kth IO, i.e., ith RIS out-phased with the kth plain IO, we have the following reflection phase: $\theta_i(t) = -2\pi f_{R,i}t + \psi_i + 2\pi f_{I,k}t - \phi_k \pmod{2\pi}$ for $i = 1, 2, \ldots, N$ and $k = 1, 2, \ldots, M$. Considering these given reflection phases, for each time instant, we search for all possible N-permutations of M plain IOs to maximize the absolute value of the complex envelope. Then, the permutation of IOs that maximizes the complex envelope magnitude is selected. This method requires a search over $P(M,N)$ permutations in each time instant, in return, has a higher complexity than the first one. Specifically, let us denote the nth permutation (the set of IOs) by $\mathcal{P}_n = \{\mathcal{P}_n^1, \mathcal{P}_n^2 \ldots, \mathcal{P}_n^N\}$ for $n = 1, 2, \ldots, P(M,N)$. For a given time instant $t = t_0$, considering all permutations, we construct the possible the set of RIS phases as $\theta_i(t_0) = -2\pi f_{R,i}t_0 + \psi_i + 2\pi f_{I,\mathcal{P}_n^i}t_0 - \phi_{\mathcal{P}_n^i} \pmod{2\pi}$ for $i = 1, 2, \ldots, N$ and the corresponding estimate of the received signal sample $r_n(t_0)$ is obtained from (S9) for the nth permutation. Finally, the optimum permutation is obtained as $\hat{n} = \arg\max_n |r_n(t_0)|$. Then, the optimal set of plain IOs to be targeted by RISs are determined as $\mathcal{P}_{\hat{n}}$ and the RIS reflection phases are adjusted accordingly: $\hat{\theta}_i(t_0) = -2\pi f_{R,i}t_0 + \psi_i + 2\pi f_{I,\mathcal{P}_{\hat{n}}^i}t_0 - \phi_{\mathcal{P}_{\hat{n}}^i} \pmod{2\pi}$ for $i = 1, 2, \ldots, N$. These procedures are repeated for all time instants. Obviously, this strategy requires the knowledge of all Doppler phases at a central processing unit, estimation of the received complex envelope samples, and a dynamic control of all RISs.
- Method 3: This method uses the same exhaustive search approach of Method 2, however, instead of maximizing the the absolute value of the complex envelope, we try to minimize the variation of it with respect to time by assigning the RISs to IOs with this purpose. Specifically, for a given time instant

$t = t_0$, the optimal permutation $\mathcal{P}_{\hat{n}}$ is obtained as $\hat{n} = \arg\min_n \big|\, |r_n(t_0)| - |r(t_{-1})| \,\big|$, where $r(t_{-1})$ is the sample of the received signal at the previous time instant, while at $t = 0$, we determine the optimal permutation as in Method 2. This method directly targets to eliminate fade patterns of the complex envelope instead of focusing on the maximization of the received signal strength by aligning (co-phasing) RISs with certain IOs. In other words, Method 3 eliminates the variations in the received signal stemming from different Doppler shifts of the incoming signals.

1.4.2 Setup II ($N > M$)

In this setup, we have more number of RISs than the plain IOs, and consequently, have much more freedom in the system design. Here, we consider the same three methods discussed above (Setup I) for the adjustment of RIS reflection phases, however, slight modifications are performed for Methods 2 and 3 due to fewer number of plain IOs in this setup. In Method 1, we align the existing RISs to the LOS path as in Setup I. To reduce the Doppler spread by Method 2, we search for all possible M-permutations of RISs to target plain IOs, i.e., a total of $P(N, M)$ permutations are considered. More specifically, at each time instant, we consider all possible RIS permutations to eliminate the reflections from M plain IOs, while the remaining $N - M$ RISs are aligned to the LOS path. The permutation of RISs that maximizes the absolute value of the sample of the received signal is selected. On the other hand, Method 3 aims to minimize the variations in $r(t)$ by assigning M RISs to M plain IOs, while also aligning the remaining $N - M$ RISs to the LOS path. Our methodology has been summarized as follows:

- Method 1: The same as Method 1 for Setup I.
- Method 2: Let us denote the nth permutation (the set of RISs) by $\mathcal{R}_n = \left\{\mathcal{R}_n^1, \mathcal{R}_n^2 \ldots, \mathcal{R}_n^M\right\}$ and the set of RISs that are not included in the nth permutation by $\mathcal{S}_n = \left\{\mathcal{S}_n^1, \mathcal{S}_n^2 \ldots, \mathcal{S}_n^{N-M}\right\}$, i.e., $\mathcal{P}_n \cup \mathcal{S}_n = \{1, 2, \ldots, N\}$ for $n = 1, 2, \ldots, P(N, M)$. For a given time instant $t = t_0$, considering all permutations, we construct the possible the set of RIS phases to eliminate IO reflections as $\theta_{\mathcal{R}_n^i}(t_0) = -2\pi f_{R,\mathcal{R}_n^i} t_0 + \psi_{\mathcal{R}_n^i} + 2\pi f_{I,i} t_0 - \phi_i \pmod{2\pi}$ for $i = 1, 2, \ldots, M$, while aligning the remaining $N-M$ RISs to the LOS path as follows: $\theta_{\mathcal{S}_n^i}(t_0) = -2\pi f_{R,\mathcal{S}_n^i} t_0 + \psi_{\mathcal{S}_n^i} - 2\pi f_D t_0 \pmod{2\pi}$ for $i = 1, 2, \ldots, N - M$. Then, the corresponding estimate of the received signal sample $r_n(t_0)$ is obtained from (S9) for the nth permutation. Finally, the optimum permutation is obtained as $\hat{n} = \arg\max_n |r_n(t_0)|$. Then, the optimal set of RISs to be paired with IOs and aligned to the LOS path are determined as $\mathcal{R}_{\hat{n}}$ and $\mathcal{S}_{\hat{n}}$, respectively, and the RIS reflection phases are adjusted accordingly: $\hat{\theta}_{\mathcal{R}_{\hat{n}}^i}(t_0) = -2\pi f_{R,\mathcal{R}_{\hat{n}}^i} t_0 + \psi_{\mathcal{R}_n^i} + 2\pi f_{I,i} t_0 - \phi_i \pmod{2\pi}$ for $i = 1, 2, \ldots, M$ and $\hat{\theta}_{\mathcal{S}_{\hat{n}}^i}(t_0) = -2\pi f_{R,\mathcal{S}_{\hat{n}}^i} t_0 + \psi_{\mathcal{S}_{\hat{n}}^i} - 2\pi f_D t_0 \pmod{2\pi}$ for $i = M+1, M+2, \ldots, N$. The above procedures are repeated for all time samples.
- Method 3: This method follows the same procedures as that of Method 2, except the determination of the optimum permutation. This is performed by $\hat{n} = \arg\min_n \big|\, |r_n(t_0)| - |r(t_{-1})| \,\big|$ considering the current (estimated corresponding to the nth permutation) and previously received signal samples of $r_n(t_0)$ and $r(t_{-1})$.

To illustrate the potential of our methods, we consider the 2D geometry of **Figure S7** in our computer simulations, where the MS and the BS are located at $(0, 0)$ and $(-1000, 0)$ in terms of their (x, y)-coordinates, respectively. We assume that $R = 10$ IOs are uniformly distributed in a predefined rectangular area at the right hand side of the origin. We again consider a mobile speed of $V = 10$ m/s with $f_c = 3$ GHz and a sampling time of $\lambda/32$, but use the following new simulation parameters: a travel distance of $30\lambda = 3$ m and an FFT size of 1024.

Table S1. Comparison of Methods 1-3 in terms of peak-to-peak variation (Δ_r in dB) and time-average ($\bar{r}$ in dB) of $|r(t)|$.

	Method 1	Method 2	Method 3
$N = 3$, $M = 7$	$\Delta_r = 11.78$ $\bar{r} = -47.22$	$\Delta_r = 5.43$ $\bar{r} = -47.76$	$\Delta_r = 3.95$ $\bar{r} = -50.17$
$N = M = 5$	$\Delta_r = 7.08$ $\bar{r} = -45.99$	$\Delta_r = 3.09$ $\bar{r} = -49.93$	$\Delta_r = 2.47$ $\bar{r} = -50.88$
$N = 7$, $M = 3$	$\Delta_r = 2.91$ $\bar{r} = -44.90$	$\Delta_r = 1.05$ $\bar{r} = -46.20$	$\Delta_r = 0.66$ $\bar{r} = -46.62$

In **Figure S8**, we investigate two extreme cases: $N = 0, M = 10$ and $N = 10, M = 0$. For the case of $N = 0, M = 10$, i.e., the case without any RISs, we observe a Doppler spectrum consisting of many components and in return, a severe deep fading pattern in the time domain. On the contrary, for the case of $N = 10, M = 0$, in which all IOs in the system are equipped with RISs, we have a full control of the propagation environment by applying Method 1 (aligning the reflected signals from all RISs to the LOS path) and observe a constant magnitude for the complex envelope as in subsection 2.2. Here, we may readily state that the case of $N = 10, M = 0$ with Method 1 provides the maximum magnitude for the complex envelope and can be considered as a benchmark for all setups/methods with $M > 0$.

In **Figures S9-S11**, we consider three different scenarios based on the number of RISs in the system: $N = 3, M = 7$ (Setup I), $N = M = 5$ (Setup I), and $N = 7, M = 3$ (Setup II) and assess the potential of the introduced Methods 1-3. As seen from **Figures S9-S11**, although Method 1 ensures a high complex envelope magnitude in average with the price of a larger Doppler spread (faster variation in time), Methods 2 and 3 are more effective in reducing the fade patterns observed in the time domain by modifying the Doppler spectrum through the elimination of plain IO signals. Particularly, the improvements provided by Method 3 are more noticeable both in time and frequency domains. For instance, for the case of $N = 7, M = 3$, Method 3 almost eliminates all Doppler spectrum components stemming from three plain IOs and ensures an approximately constant magnitude for the complex envelope, as seen from **Figure S11**.

To gain further insights, in Table S1, we provide a quantitative analysis by comparing the peak-to-peak value Δ_r of $|r(t)|$ and its time average $\bar{r}$ (both measured in dB) for all methods, i.e., $\Delta_r = |r(t)|_{\max} - |r(t)|_{\min}$ and $\bar{r} = \frac{1}{n_s}\sum_{n=0}^{n_s-1} |r(it_s)|$, where n_s and t_s respectively stand for the total number of time samples and sampling time, which are selected as $n_s = 960$ and $t_s = 0.3125$ ms for this specific simulation. As observed from Table S1, increasing N noticeably reduces Δ_r for all methods, while this reduction is more remarkable for Methods 2 and 3. We also evince that Methods 2 and 3 cause in a slight degradation in $\bar{r}$ since they utilize RISs to cancel out reflections from plain IOs. Generalizing our discussion from Subection 4.2.1, we claim that Method 1 can be the preferred choice to maximize the (time-averaged) magnitude of the complex envelope due to the stronger LOS path, however, the complete mathematical proof of this claim is highly intractable. We also observe that Method 2 provides a nice compromise between Methods 1 and 3 by providing a much lower Δ_r with a close $\bar{r}$ compared to Method 1, while Method 3 ensures the minimum Δ_r.

1.5 The General Case with Multiple IOs and without the Direct Signal

In this section, we revisit the general case of the previous section (**Figure S6**), however, without the presence of a LOS path. For this case, the received signal with N RISs and M plain IOs can be expressed as follows:

$$r(t) = \frac{\lambda}{4\pi}\left(\sum_{i=1}^{N}\frac{e^{j2\pi f_{R,i}t - j\psi_i + j\theta_i(t)}}{\tilde{d}_{R,i}} - \sum_{k=1}^{M}\frac{e^{j2\pi f_{I,k}t - j\phi_k}}{\tilde{d}_{I,k}}\right). \tag{S10}$$

Here, the three methods introduced in Supplementary subsection 1.4 can be applied with slight modifications. For Method 1, since there is no LOS path, the available RISs in the system can be aligned to the strongest path, which might be from either an RIS or a plain IO and has the shortest radio path distance. For Methods 2 and 3, when $M \geq N$, we use the same procedures as in the LOS case and assign all N RISs to the plain IOs with different purposes. However, when $N > M$, after applying the same permutation selection procedures, we determine the RIS with the strongest path among the remaining $N - M$ RISs in lieu of the LOS path and align the rest of the RISs ($N - M - 1$ ones) to this strongest RIS for each specific permutation. Our methodology has been summarized below:

1.5.1 Setup I ($\boldsymbol{M \geq N}$)

- Method 1: We align the existing N RISs to the strongest path. If the strongest path belongs to a RIS, whose index is a, we have $\theta_i(t) = -2\pi f_{R,i}t + \psi_i + 2\pi f_{R,a}t - \psi_a \pmod{2\pi}$ for $i = 1, \ldots, a-1, a+1, \ldots, N$, while $\theta_a(t) = 0$. Otherwise, if the strongest path belongs to a plain IO with index a, we have $\theta_i(t) = -2\pi f_{R,i}t + \psi_i + 2\pi f_{I,a}t - \phi_a + \pi \pmod{2\pi}$ for $i = 1, 2, \ldots, N$. Please note that $a = \arg\min_i \tilde{d}_{R,i}$ if $\min_i \tilde{d}_{R,i} < \min_k \tilde{d}_{I,k}$ or $a = \arg\min_k \tilde{d}_{I,k}$, otherwise.
- Method 2: The same as Method 2 in Supplementary subsection 1.4 for $M \geq N$ except that $r_n(t_0)$ is obtained from (S10) for the nth permutation.
- Method 3: The same as Method 3 in Supplementary subsection 1.4 for $M \geq N$ except that $r_n(t_0)$ is obtained from (S10) for the nth permutation.

1.5.2 Setup II ($\boldsymbol{N > M}$)

- Method 1: The same as Method 1 given above.
- Method 2: We follow the same steps for Method 2 in subsection 1.4 for $N > M$, however, for nth permutation, the strongest RIS is selected among the set $\mathcal{S}_n$ (the set of $N - M$ RISs that are not included in the elimination of IO reflections). Denoting the index of this strongest RIS by a_n, where $a_n = \arg\min_{i \in \mathcal{S}_n} \tilde{d}_{R,i}$, we have $\theta_{\mathcal{S}_n^i}(t_0) = -2\pi f_{R,\mathcal{S}_n^i} t_0 + \psi_{\mathcal{S}_n^i} + 2\pi f_{R,a_n} t_0 - \psi_{a_n} \pmod{2\pi}$ for $i = 1, 2, \ldots, N - M$ with $\mathcal{S}_n^i \neq a_n$ and $\theta_{a_n}(t_0) = 0$ for this case. The above procedures are repeated for all permutations and the estimates of the received signal samples are obtained as $r_n(t_0)$ from (S10) for $n = 1, 2, \ldots, P(N, M)$. After the determination of the optimal permutation $\hat{n}$, we obtain the set of RISs targeting the IOs as $\mathcal{R}_{\hat{n}}$ while the set of remaining RISs are given by $\mathcal{S}_{\hat{n}}$. Finally, RIS angles are determined as in Method 2 in subsection 1.4 for $N > M$ with the exception that the phases of the remaining $N - M$ RISs are aligned as $\hat{\theta}_{\mathcal{S}_{\hat{n}}^i}(t_0) = -2\pi f_{R,\mathcal{S}_{\hat{n}}^i} t_0 + \psi_{\mathcal{S}_{\hat{n}}^i} + 2\pi f_{R,a_{\hat{n}}} t_0 - \psi_{a_{\hat{n}}} \pmod{2\pi}$ for $i = 1, 2, \ldots, N - M$ with $\mathcal{S}_{\hat{n}}^i \neq a_{\hat{n}}$ and $\hat{\theta}_{a_{\hat{n}}}(t_0) = 0$. The above procedures are repeated for all time instants.
- Method 3: This method follows the same procedures as that of Method 2 given above, except the determination of the optimum permutation, which is discussed in Supplementary subsection 1.4.

In **Figures S12,S13**, we investigate the application of Methods 1-3 in two scenarios: $N = 3, M = 7$ (Setup I) and $N = 7, K = 3$ (Setup II) for the same simulation scenario of **Figure S7** by ignoring the LOS path. Compared to **Figures S9,S11**, we observe that due to the nonexistence of the LOS path, all methods

provide a similar level of time-average ($\bar{r}$) for the complex envelope while Methods 2 and 3 eliminate deep fades in the received signal. In other words, since we do not have a stronger LOS path, Method 1 loses its main advantage in terms of $\bar{r}$ compared to the other two methods for both scenarios.

It is worth noting that for the case of $N = 0$, none of the methods are applicable as in the case of the previous section. However, for $M = 0$, Doppler effect can be totally eliminated due to the nonexistence of the LOS path as follows: $\theta_i(t) = -2\pi f_{R,i}t + \phi_i \pmod{2\pi}$ for $i = 1, 2, \ldots, N$.

As a final note, our aim here is to find heuristic solutions to mitigate deep fading and Doppler effects under arbitrary number of RISs and plain IOs, and the determination of the ultimately optimum RIS angles are beyond the scope of this work. Although our methods provide satisfactory results, there might be a certain permutation of RISs/IOs with specific reflection phases that may guarantee a maximized received complex envelope magnitude and/or the lowest Doppler spread. However, the theoretical derivation of this ultimate optimal solution seems intractable at this moment.

2 PRACTICAL ISSUES

In this supplementary section, we consider a number of practical issues and investigate the performance of our solutions under certain imperfections in the system.

2.1 Realistic RISs

Throughout this paper, we assumed that the utilized RISs have a unit-amplitude reflection coefficient with a very high resolution reflection phase $\theta(t) \in [0, 2\pi)$ that can be tuned in real time. However, as reported in recent studies, there can be not only a dependency between the amplitude and the phase but also a limited range can be supported for the reflection phase. For this purpose, we consider the realistic RIS design of Tretyakov *et al.* (Liu et al., 2019), which has a reflection amplitude of -1 dB with a reflection phase between -150° and 140°. In **Figure S14**, we compare the complex envelope magnitudes of two scenarios in the presence of a perfect RIS (P-RIS) and an imperfect RIS (I-RIS) with practical constraints: i) the scenario of **Figure 1** with $N = 1, M = 0$ and ii) the scenario of **Figure S1** with $N = M = 1$. As seen from **Figure S14**, the practical RIS of (Liu et al., 2019) causes a slight degradation both in magnitude and shape of the complex envelope, however, its overall effect is not significant. A further degradation would be expected in the presence of discrete phase shifts (Wu and Zhang, 2019), and this analysis is left for interested readers.

2.2 Imperfect Knowledge of Doppler Frequencies

As discussed in Supplementary section 1, in case of multiple RISs, a central processing unit needs to acquire the knowledge of Doppler frequencies of all incoming rays to initiate Methods 1-3 in coordination with the available RISs. Here, we assume that due to erroneous estimation of the velocity of the MS and/or relative positions of the IOs, the RISs in the system are fed back with erroneous Doppler shifts (in Hz), given by $f^e_{R,i} = f_{R,i} + e_{R,i}$ and $f^e_{I,k} = f_{I,k} + e_{I,k}$, while the dominant Doppler shift (f_D) stemming from the LOS path is perfectly known. Here, $e_{R,i}$ and $e_{I,k}$ respectively stand for the errors in Doppler shifts for ith RIS and kth plain IO. To illustrate the effect of this imperfection, these estimation error terms are modelled by independent and identically distributed uniform random variables in the range $[-U, U]$ (in Hz). In **Figure S15**, we consider the scenario of $N = 7, M = 3$ with $U = 0$, 1 and 3 for the same geometry of **Figure S7**. As seen from **Figure S15**, while the degradation in the complex envelope is not a major concern for $U = 1$, a significant distortion has been observed for the case of $U = 4$ with respect to time. Here,

Methods 2 and 3 appear more reliable in the presence of Doppler frequency estimation errors, however, we observe that the overall system is highly sensitive to this type of error.

We note that the estimation of Doppler frequencies and/or real-time adaptation of RISs in realistic channel conditions are interesting research problems to be investigated with the framework of RIS-empowered systems.

2.3 High Mobility & Discrete-Time RIS Phases

In this subsection, we will focus on the case of high mobility under the assumption of discrete-time RIS reflection phases. In this scenario, the RIS reflection phases remain constant for a certain time duration. It is worth noting that all methods described earlier are also valid for the case of high mobility if the RIS reflection phases can be tuned in real-time with a sufficiently high rate. However, in practice, due to limitations in terms of the RIS design and signaling overhead in the network, the RIS reflection phases can be tuned at only (certain) discrete-time instants. Let us denote the RIS reconfiguration interval by t_r (in seconds), i.e., the RIS phases can be adjusted in every t_r seconds only. In our first computer simulation, we consider that the complex envelope is represented by its samples taken at every t_s seconds. Here, we assume that once the RIS reflection phases are adjusted according to the LOS path, they remain fixed for Qt_s seconds. In other words, for $Q = 1$, we update the RIS reflection phases at each sampling time and obtain the results given throughout the paper. In **Figure S16A**, we perform this simulation for the high mobility case of $V = 100$ m/s, $f_c = 3$ GHz and $t_s = 3.125$ μs with $N = 1$ and $M = 0$ (for the basic scenario of **Figure 1**). Here, t_s has been intentionally reduced to capture the variations in the complex envelope with respect to time due to the higher Doppler spread of the unmodulated carrier and a travel distance of 3λ is considered. In this case, we assume that RIS reflection phases are modified as $\theta(t) = -4\pi f_D t \pmod{2\pi}$ in every Qt_s seconds, i.e., the RIS cannot be reconfigured fast enough compared to the sampling frequency (variation) of the complex envelope. As seen from **Figure S16A**, a distortion is observed in the complex envelope due to the delayed reconfiguration of RIS reflection phases. However, we conclude that even if with $Q = 50$, the variation in the complex envelope is not as significant as in the case without an RIS (shown in the figure as a benchmark), while the variation is not significant for $Q = 20$. In what follows, we present a theoretical framework to describe this phenomenon.

In mathematical terms, for the considered scenario that is formulated by (4) in terms of its received complex envelope, assuming that the RIS reflection phase is adjusted and fixed at time instant t_1 while focusing on the complex envelope at time $t_2 > t_1$, we obtain

$$\begin{aligned} r(t_2) &= \frac{\lambda}{4\pi}\left(\frac{e^{-j2\pi f_D t_2}}{d_{\text{LOS}}} + \frac{e^{j2\pi f_D t_2 + j\theta(t_1)}}{d_{\text{LOS}} + 2d_1}\right) \\ &= \frac{\lambda e^{-j2\pi f_D t_2}}{4\pi}\left(\frac{1}{d_{\text{LOS}}} + \frac{e^{j4\pi f_D \Delta t}}{d_{\text{LOS}} + 2d_1}\right) \end{aligned} \tag{S11}$$

where $\Delta t = t_2 - t_1 < t_r$. Here, we considered the fact that the RIS reflection phase is fixed at time t_1 as $\theta(t_1) = -4\pi f_D t_1$. As a result, we observe a variation in the complex envelope magnitude, which is a function of both f_D and Δt. It is worth noting that letting $\Delta t = 0$ in (S11), one can obtain (5) for $t = t_2$. After simple manipulations, the magnitude of the complex envelope is calculated as

$$|r(t_2)| = \left(\frac{\lambda}{4\pi}\right)\left(\frac{1}{d_{\text{LOS}}^2} + \frac{1}{(d_{\text{LOS}} + 2d_1)^2} + \frac{2\cos(4\pi f_D \Delta t)}{d_{\text{LOS}}(d_{\text{LOS}} + 2d_1)}\right)^{1/2}. \tag{S12}$$

It is evident from (S12) that the magnitude of the complex envelope is no longer constant unless $4\pi f_D \Delta t \ll 1$. In light of the above analysis, to ensure a constant magnitude for the complex envelope, that is, to eliminate the fade pattern due to Doppler spread, we must have $t_r < \frac{1}{40\pi f_D}$ for the considered scenario. In other words, the RIS should be tuned fast enough compared to f_D to capture the variations of the received signal. To illustrate this effect, in **Figure S16B**, for a fixed t_r value of 12.5 μs, we change the velocity of the MS and observe the magnitude of the complex envelope. As seen from **Figure S16B**, while the smaller Doppler frequency of 500 Hz ($V = 50$ m/s) can be captured by the RIS since $t_r < \frac{1}{40\pi f_D} = 15.91$ μs for this scenario, we observe an oscillation in the magnitude for the higher Doppler frequencies of 2 kHz ($V = 200$ m/s) and 4 kHz ($V = 400$ m/s) since the condition of $t_r < \frac{1}{40\pi f_D}$ is no longer satisfied. In light of the above discussion, we conclude that increasing Doppler frequencies poses a much bigger challenge for the real-time adjustment of RIS reflection phases.

Finally, it is worth noting that in case of slow fading $(1/f_D \gg T_s)$, where T_s is the symbol duration, the channel may be assumed to be static over one or several transmission intervals and the variations in the magnitude of the complex envelope from symbol to symbol (in our case, for unmodulated cosine signals) can be compensated by adjusting RIS reflection phases at every T_s seconds (with slight variations in magnitude if $T_s > \frac{1}{40\pi f_D}$). On the other hand, in the case of fast fading $(1/f_D < T_s)$, since the channel impulse response changes rapidly within the symbol duration, in order to compensate Doppler and fading effects, i.e., to obtain a fixed magnitude for the complex envelope during a symbol duration, RIS reflection phases should be tuned at a much faster rate compared to T_s. As an example, consider the transmission of an unmodulated cosine signal for a period of 3 ms as in **Figure S16A**. For this case, we have fast fading due to the large Doppler spread, and this can be eliminated by adjusting the RIS reflection phases at a much faster rate compared to 3 ms, i.e., $t_r < 7.96$ μs. Failure of doing this causes variations in the complex envelope magnitude as shown in **Figure S16A**.

APPENDIX

The received complex envelope in (S2) can be expressed as

$$r(t) = r_{\text{LOS}} e^{j\xi_{\text{LOS}}(t)} + r_1 e^{j\xi_1(t)} + r_2 e^{j\xi_2(t)} \tag{S13}$$

where magnitude and phase values of the LOS and two reflected signals (from IO 1 (RIS) and IO 2) are shown by r_{LOS}, r_1, r_2 and $\xi_{\text{LOS}}(t)$, $\xi_1(t)$, $\xi_2(t)$, respectively. Here, we are interested in the maximization of $|r(t)|$ with respect to $\xi_1(t) = 2\pi f_D t + \theta_1(t)$, which captures the reconfigurable reflection phase of the RIS. We use the following trigonometric identity: For $z_1 = r_1 e^{j\xi_1}$, $z_2 = r_2 e^{j\xi_2}$, $z_3 = r_3 e^{j\xi_3}$, and $z_4 = z_1 + z_2 + z_3 = r_4 e^{j\xi_4}$, we have $r_4 = (r_1^2 + r_2^2 + r_3^2 + 2r_1 r_2 \cos(\xi_1 - \xi_2) + 2r_1 r_3 \cos(\xi_1 - \xi_3) + 2r_2 r_2 \cos(\xi_2 - \xi_3))^{1/2}$. In light of this, the maximization of $|r(t)|$ can be formulated as

$$\begin{aligned}
&\max_{\theta_1(t)} \ |r(t)|^2 \\
&\max_{\theta_1(t)} \ r_{\text{LOS}} r_1 \cos(\xi_{\text{LOS}}(t) - \xi_1(t)) + r_1 r_2 \cos(\xi_1(t) - \xi_2(t)) \\
&\max_{\theta_1(t)} \ r_{\text{LOS}} \cos(4\pi f_D t + \theta_1(t)) \\
&\qquad + r_2 \cos(2\pi f_D t(1 - \cos\alpha) + \phi_2 + \theta_1(t))
\end{aligned} \tag{S14}$$

where the constant magnitude terms and the term does not contain $\theta_1(t)$ is dropped. Using the identity $\cos(x+y) = \cos x \cos y - \sin x \sin y$ and grouping the terms with $\theta_1(t)$, we obtain

$$\begin{aligned} &\max_{\theta_1(t)} \; A\cos\theta_1(t) + B\sin\theta_1(t) \\ &\max_{\theta_1(t)} \; \mathrm{sgn}(A)\sqrt{A^2+B^2}\cos(\theta_1(t) + \tan^{-1}(-B/A)) \end{aligned} \tag{S15}$$

where A and B are as defined in (S5) and the harmonic addition theorem is used. Consequently, to maximize the complex envelope, we have to ensure

$$\mathrm{sgn}(A)\cos(\theta_1(t) + \tan^{-1}(-B/A)) = 1. \tag{S16}$$

This can be satisfied by

$$\theta_1(t) = \frac{\pi}{2}(1 - \mathrm{sgn}(A)) - \tan^{-1}(-B/A) \tag{S17}$$

which completes the proof.

REFERENCES

Goldsmith, A. (2005). *Wireless Communications* (Cambridge, UK: Cambridge University Press)

Liu, F., Tsilipakos, O., Pitilakis, A., Tasolamprou, A. C., Mirmoosa, M. S., Kantartzis, N. V., et al. (2019). Intelligent metasurfaces with continuously tunable local surface impedance for multiple reconfigurable functions. *Phys. Rev. Applied* 11, 044024

Wu, Q. and Zhang, R. (2019). Beamforming optimization for intelligent reflecting surface with discrete phase shifts. In *Proc. 2019 IEEE Int. Conf. Acoust. Speech Signal Process. (ICASSP)* (Brighton, UK)

FIGURE CAPTIONS

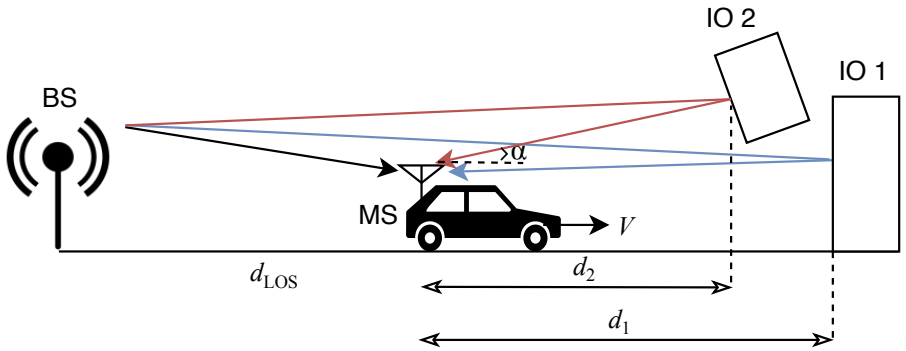

Figure S1. Propagation scenario with two IOs.

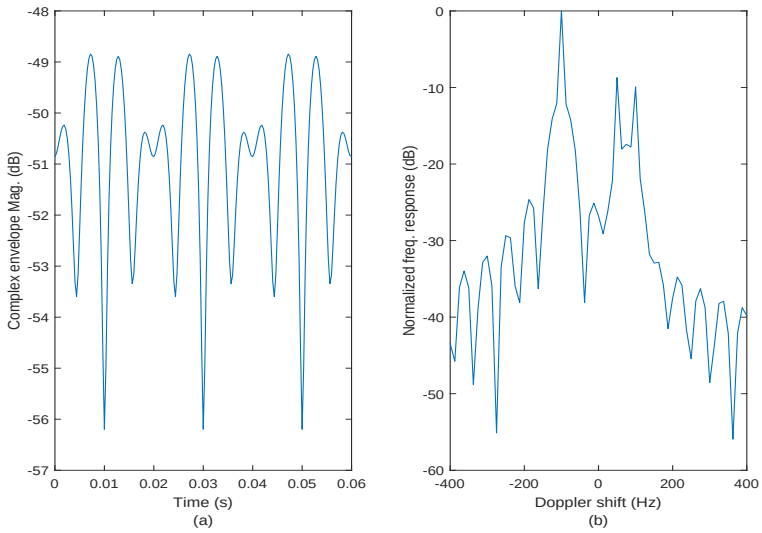

Figure S2. The scenario of **Figure S1** without an RIS: (a) Complex envelope magnitude, (b) Doppler spectrum of the received signal.

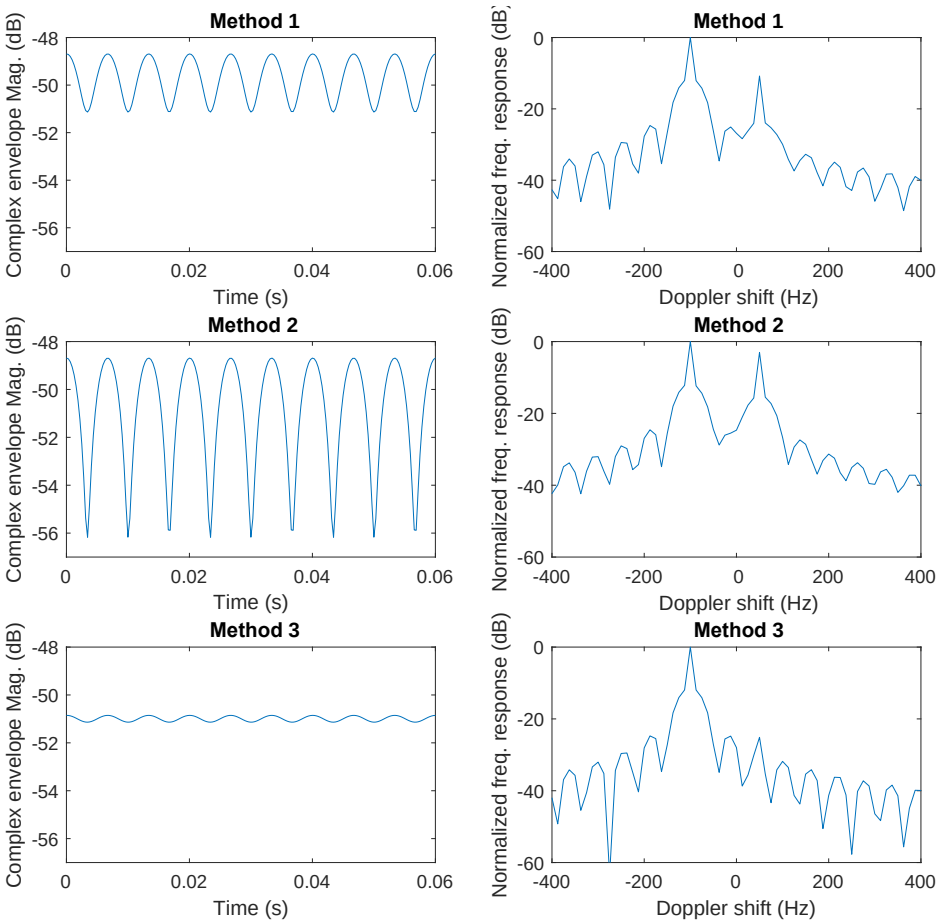

Figure S3. Magnitude and Doppler spectrum of the received signal with an RIS for scenario of **Figure S1** under three different phase selection methods.

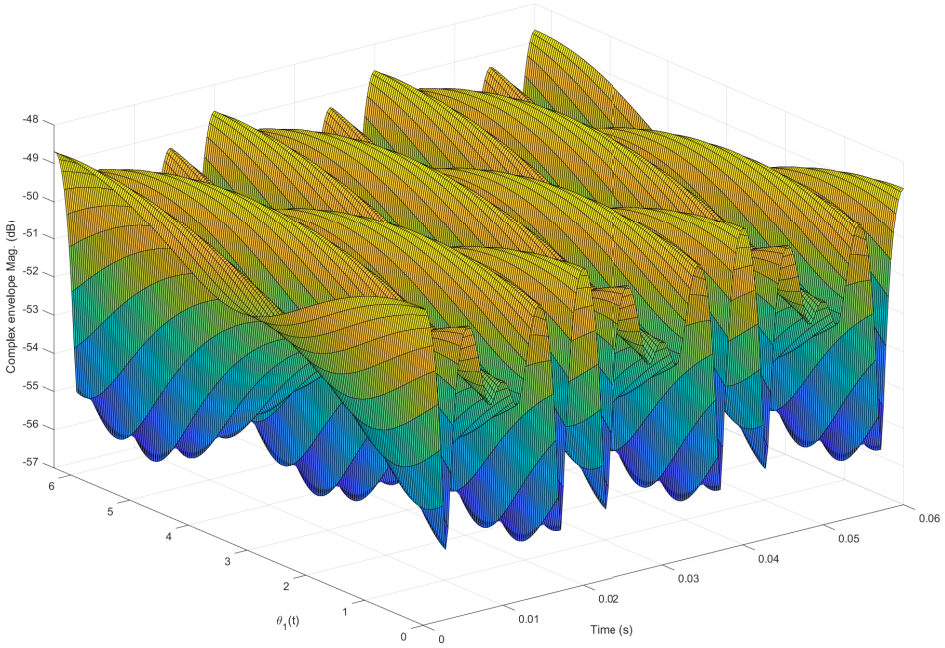

Figure S4. 3D illustration of the variation of the complex envelope magnitude with respect to time for all possible RIS reflection angles (scenario of **Figure S1**).

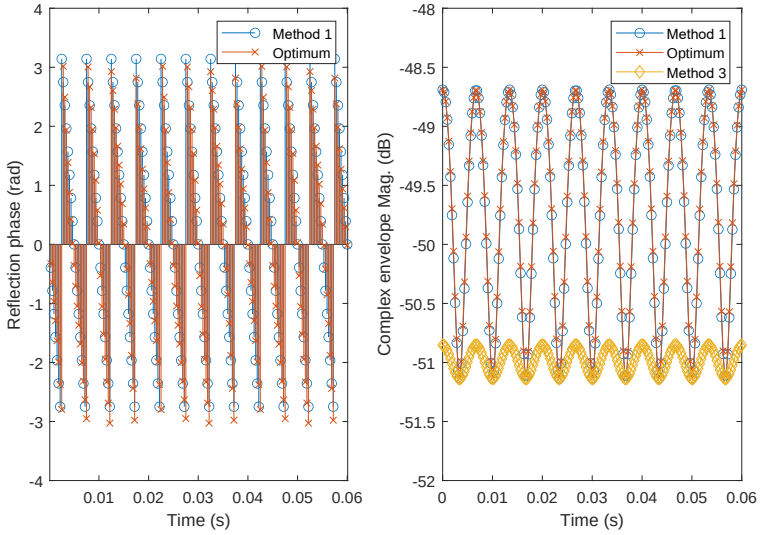

Figure S5. Comparison of reflection phases and complex envelope magnitudes for Method 1 and the optimum method.

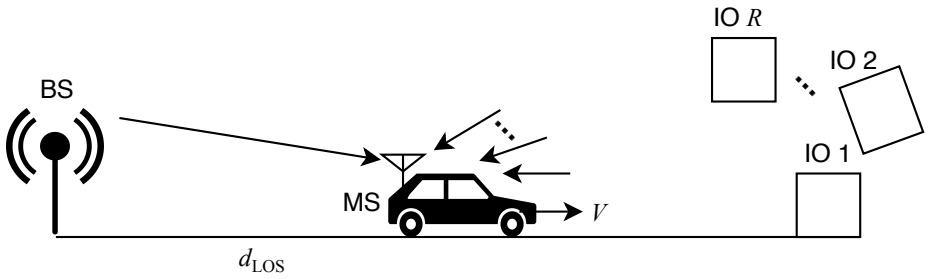

Figure S6. The general case of multiple IOs with N RISs and M plain IOs ($R = N + M$).

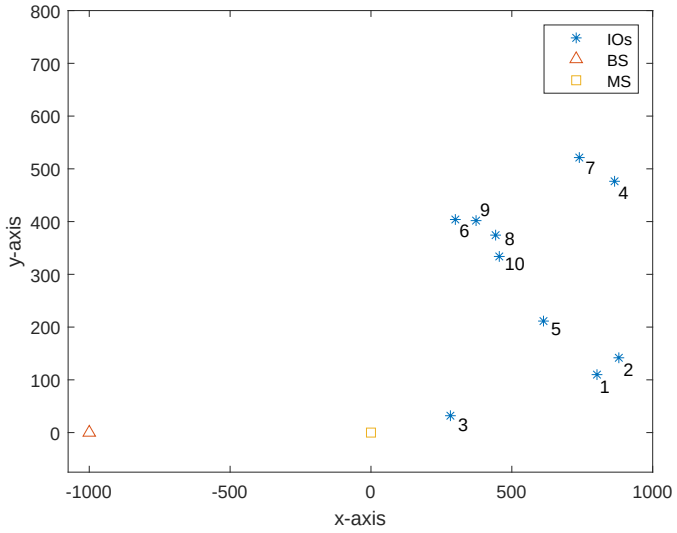

Figure S7. Considered simulation geometry with multiple IOs (the first N of them are assumed to have RISs).

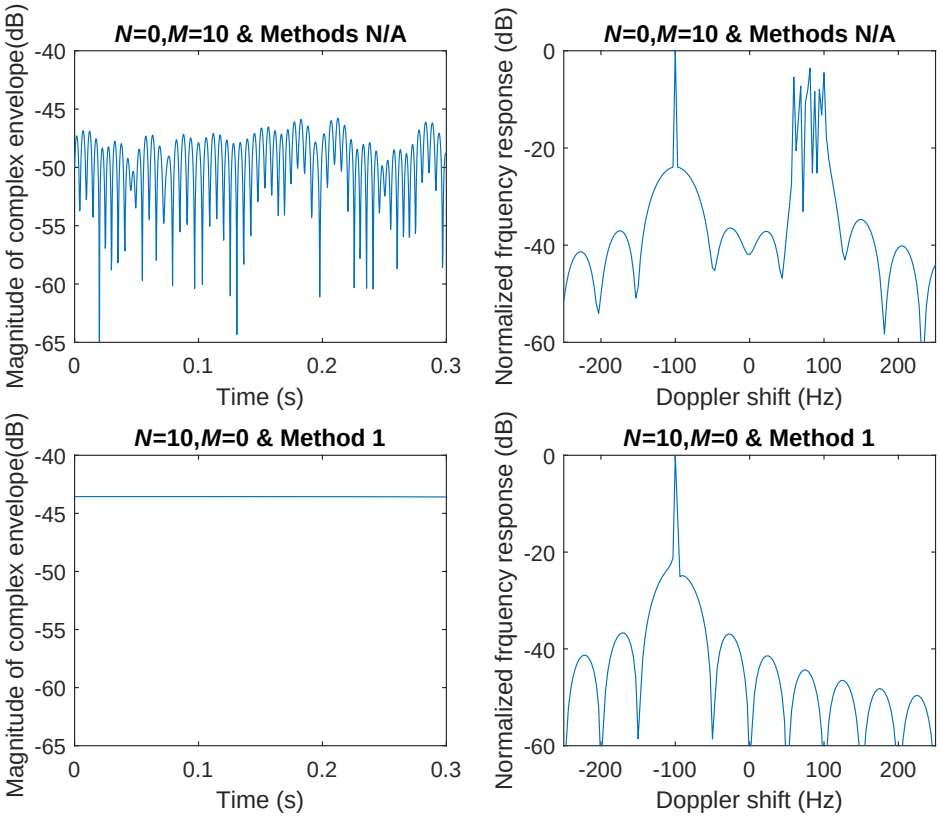

Figure S8. Complex envelope and Doppler spectrum for two extreme cases under the scenario of **Figure S6**: (top) $N = 0, M = 10$ (10 plain IOs without any RISs) and (bottom) $N = 10, M = 0$ (10 RISs without any plain IOs).

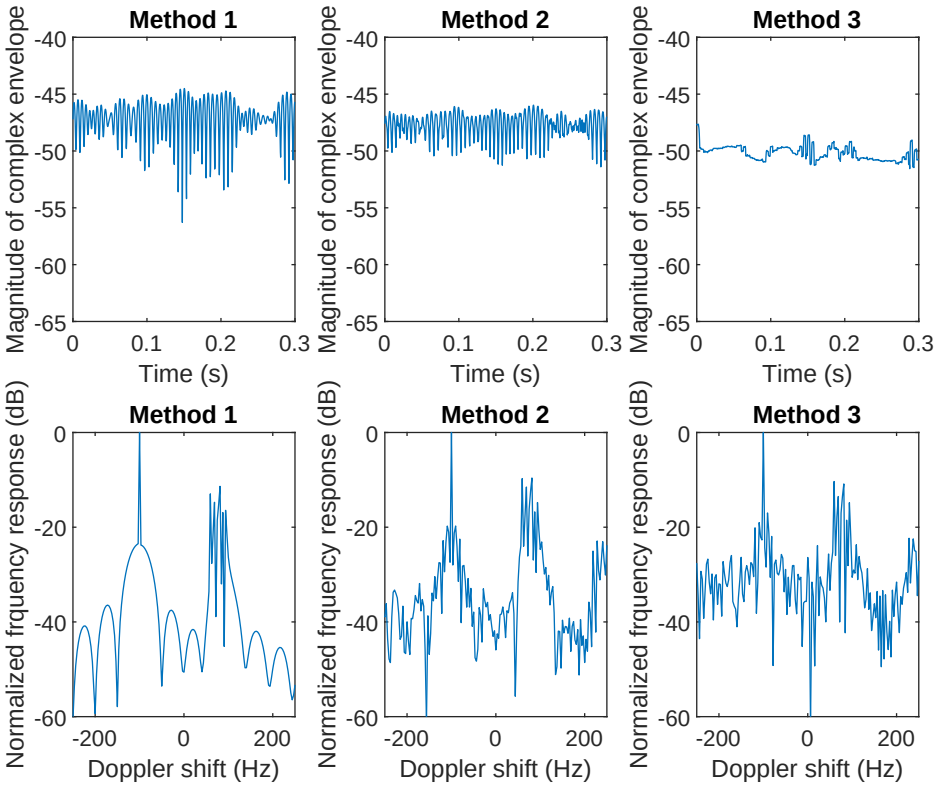

Figure S9. Complex envelope magnitude and Doppler spectrum for the general case with 10 IOs and $N = 3, M = 7$ (Setup I).

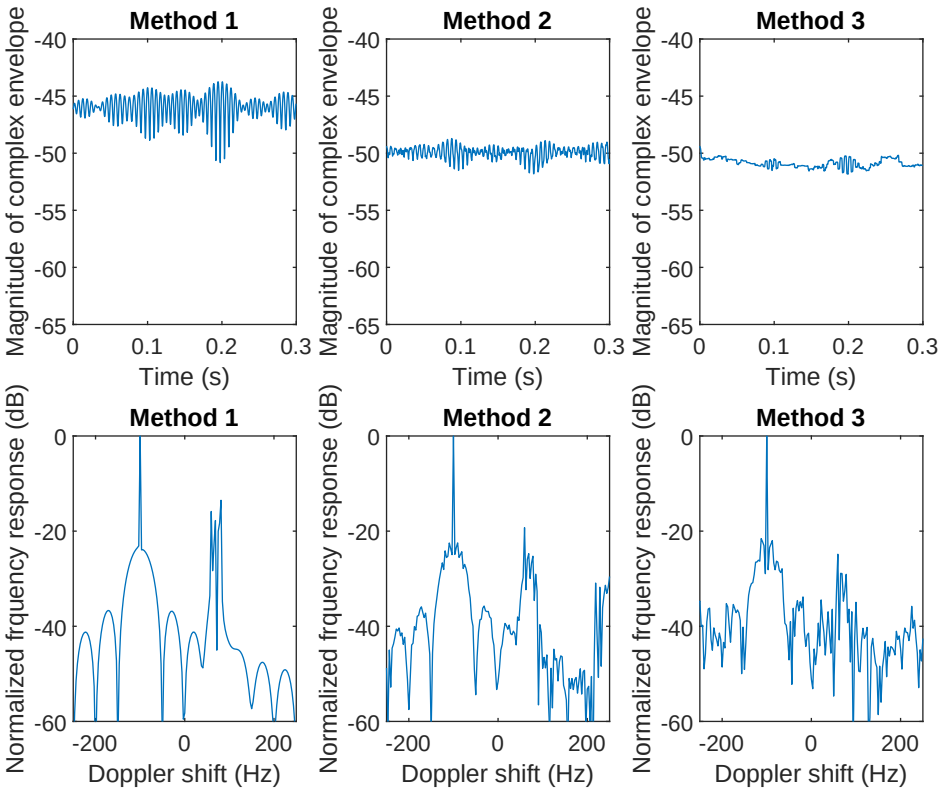

Figure S10. Complex envelope magnitude and Doppler spectrum for the general case with 10 IOs and $N = M = 5$ (Setup I).

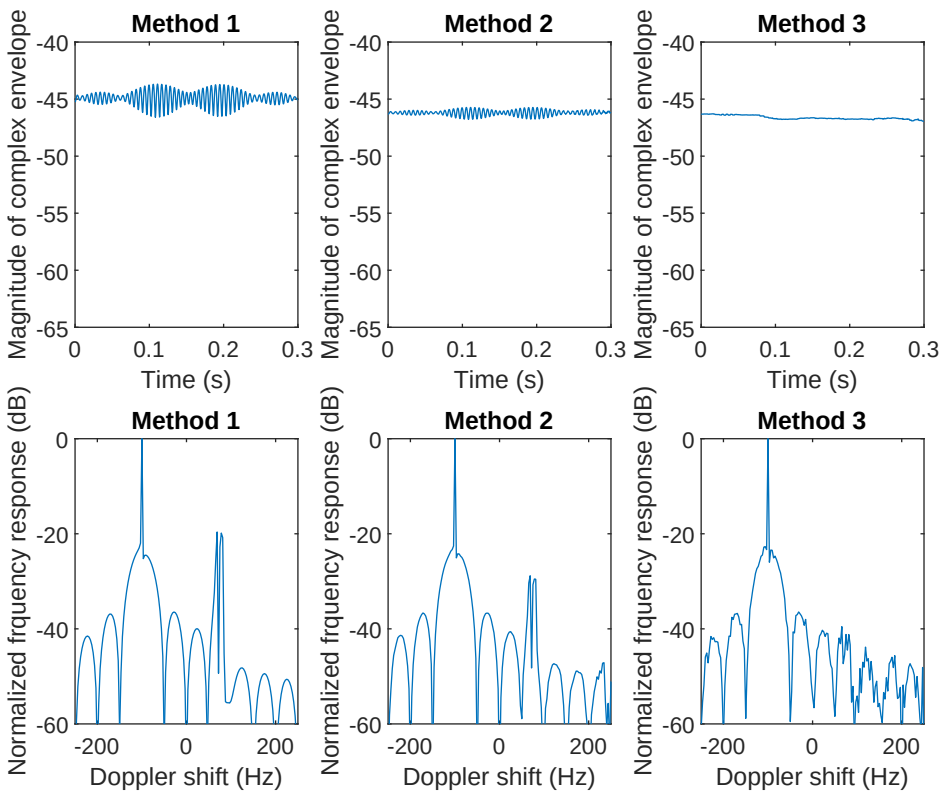

Figure S11. Complex envelope magnitude and Doppler spectrum for the general case with 10 IOs and $N = 7, M = 3$ (Setup II).

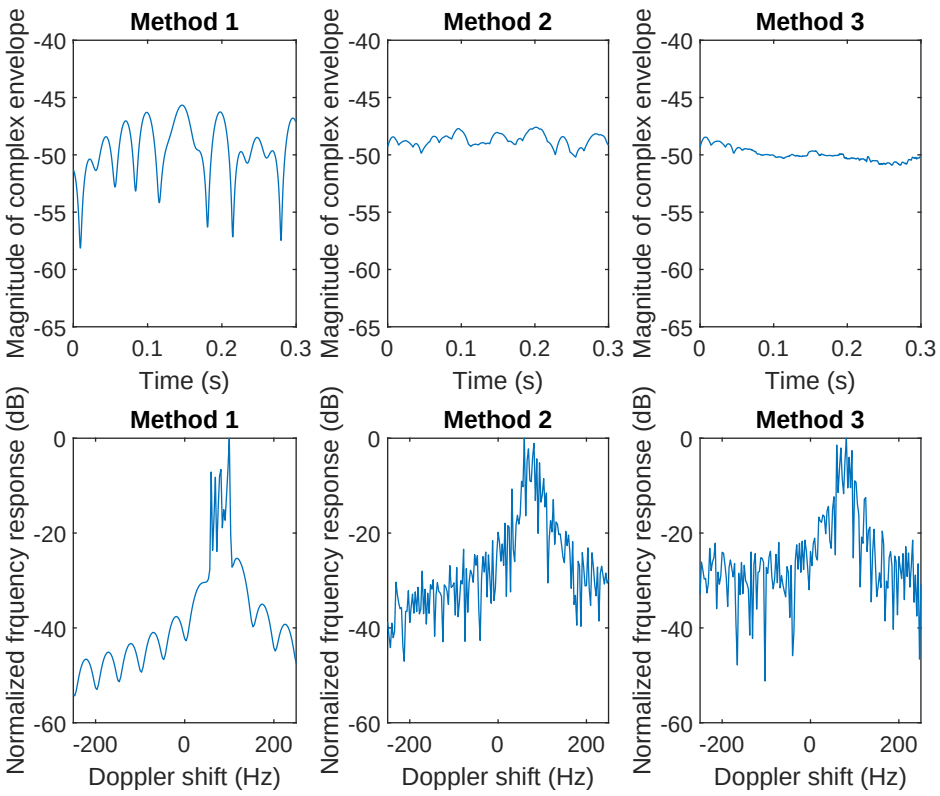

Figure S12. Complex envelope magnitude and Doppler spectrum for the general case with 10 IOs without a LOS path and $N = 3, M = 7$ (Setup I).

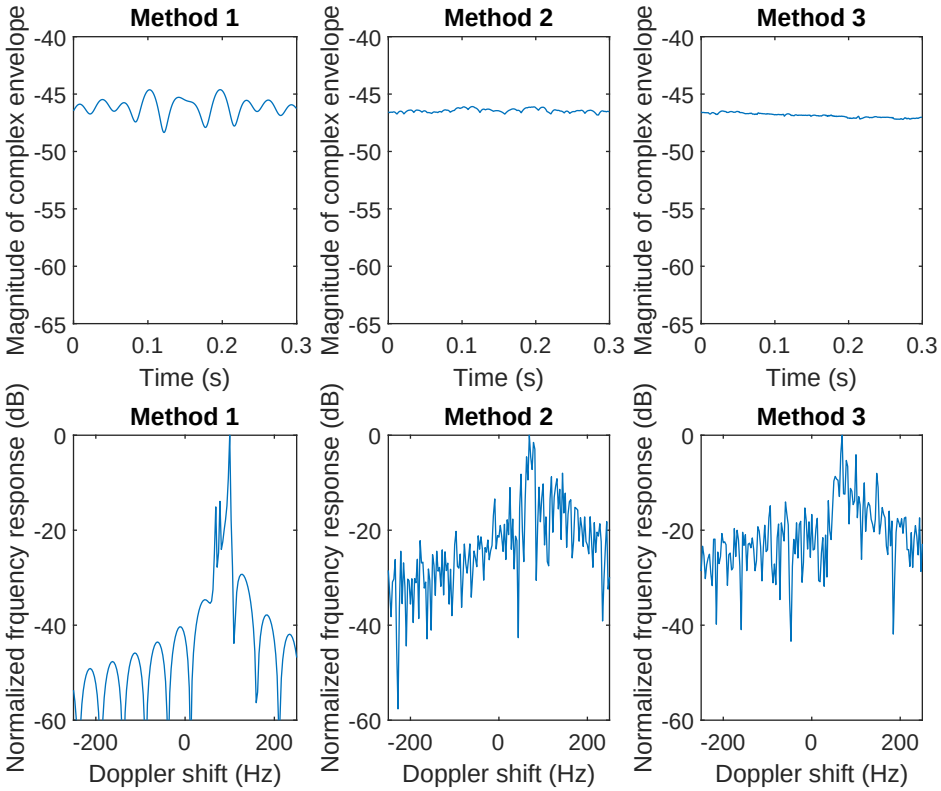

Figure S13. Complex envelope magnitude and Doppler spectrum for the general case with 10 IOs without a LOS path and $N = 7, M = 3$ (Setup II).

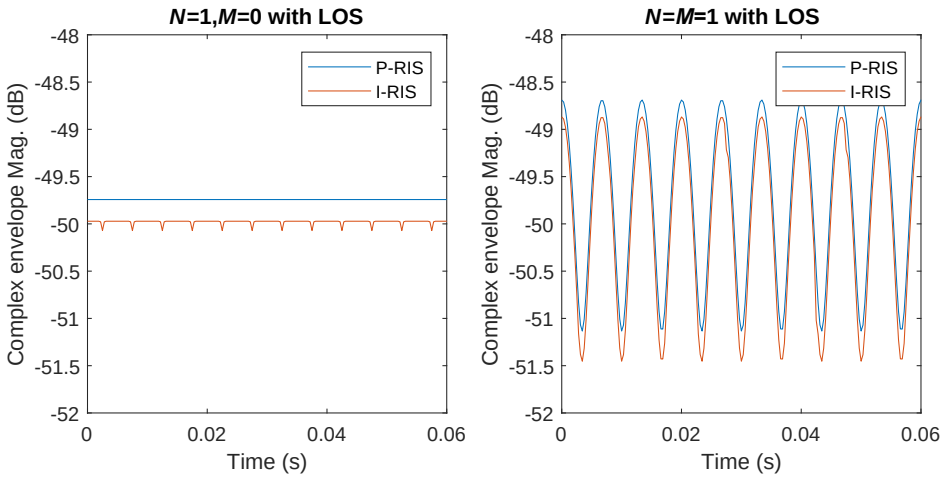

Figure S14. Complex envelope magnitude in the presence of a realistic RIS for the scenarios of **Figures 1,S1**.

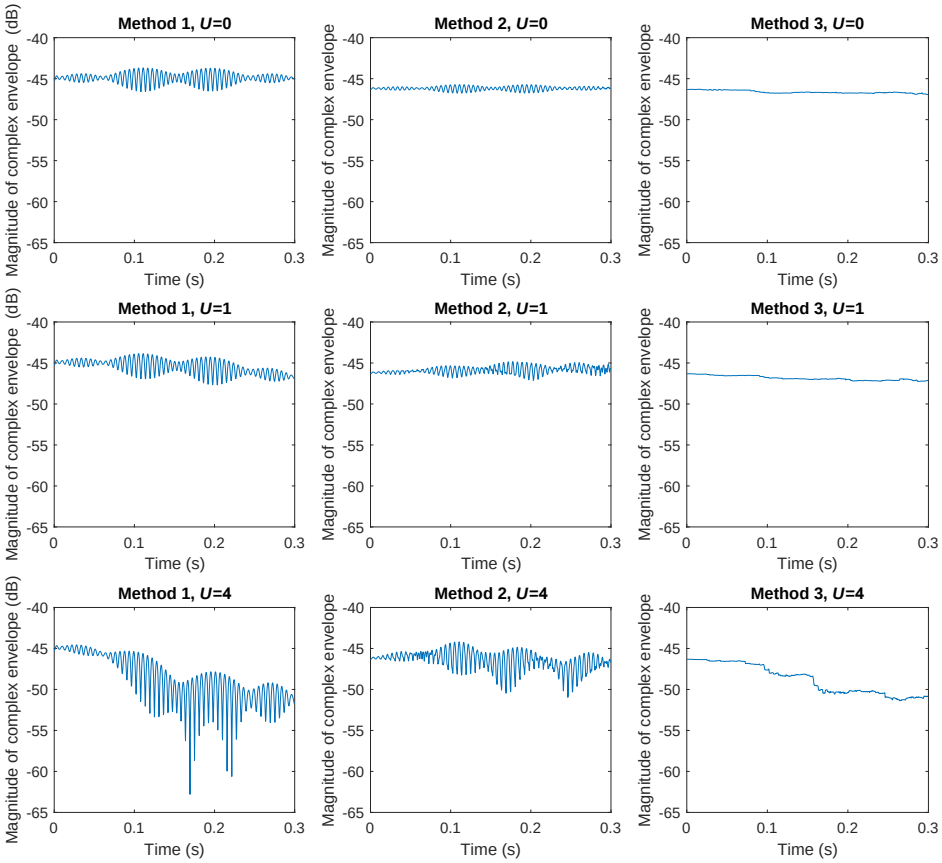

Figure S15. Complex envelope magnitude for the general case with 10 IOs with a LOS path and $N = 7, M = 3$ under erroneous Doppler frequency shifts at RISs ($U = 1$ and 4) with the perfect case ($U = 0$).

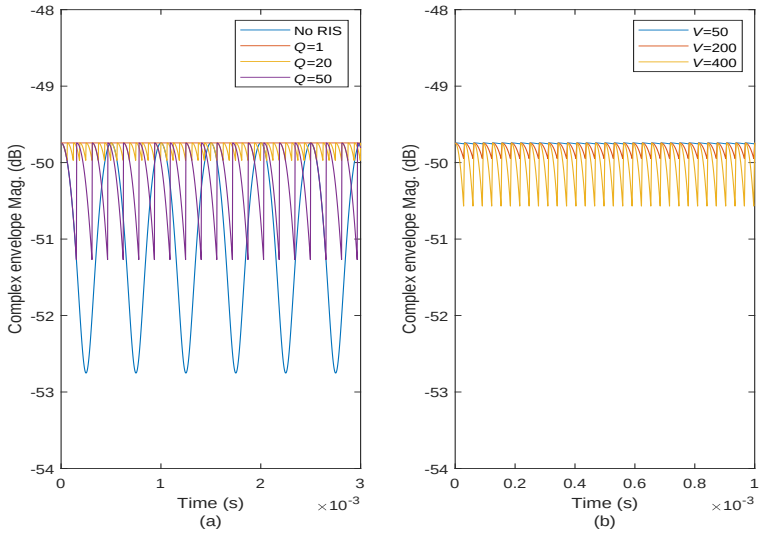

Figure S16. Complex envelope magnitude for the scenario of **Figure 1** ($N = 1, M = 0$) a) under high mobility ($V = 100$ m/s) and fixed reflection phases for a period of Qt_s seconds with $Q = 1$, 20, and 50, b) under increasing Doppler frequencies and a reflection phase update duration of $t_r = 12.5$ μs.